Biomicrofluidics ARTICLE scitation.org/journal/bmf

Optimization of a microfluidic spiral channel used to separate sperm from blood cells

Cite as: Biomicrofluidics 14, 064103 (2020); doi: 10.1063/5.0029508
Submitted: 14 September 2020 · Accepted: 25 October 2020 ·
Published Online: 5 November 2020

Sabin Nepal,[1,a)] Haidong Feng,[1] and Bruce K. Gale[1,2]

AFFILIATIONS

[1]Department of Mechanical Engineering, University of Utah, Salt Lake City, Utah 84112, USA
[2]Advanced Conceptions Inc., Salt Lake City, Utah 84108, USA

[a)]**Author to whom correspondence should be addressed:** sabinnepal@hotmail.com. **Tel.:** +1-801-347-3158

ABSTRACT

Assisted reproductive technology includes medical procedures that confront the problem of infertility. In some cases of male infertility, blood cells are present in the sperm containing samples and must be removed. Spiral-channel devices have been developed to perform this task, but there is a strong need to increase their throughput. In this work, the theory behind the separation is employed to optimize the device for increased throughput. An existing device that is known to separate sperm and blood cells with a rectangular cross section of $600 \times 100\,\mu m^2$ was used as the baseline. Using its physics, theoretical models were generated to explore theoretical performances of larger-size channels. The models suggested that a channel of size $800 \times 133\,\mu m^2$ would likely work. This geometry enabled the throughput to be increased by 50%, from 2 ml/min in the case of the baseline-size to 3 ml/min in the designed device. Experiments using the larger device resulted in a recovery of more than 90% of sperm cells while removing 89% of red blood cells (RBCs). In comparison, the reference device results in a 90% recovery of sperm cells while removing 74% of white blood cells (WBCs). The length of the channel was also reduced to reduce the pressure required to operate the chip. Literature has shown the removal of WBCs to be higher than that of RBCs due to their larger size, spherical shape, and comparatively low deformability, suggesting that the revised chip would be faster and better for the separation of sperm and all blood cells.

I. INTRODUCTION

Infertility affects 8%–12% of couples, globally, 50% of which are due to male infertility.[1] Intracytoplasmic sperm injection (ICSI), an assistive reproductive technology (ART), has revolutionized male infertility treatment by allowing as few as one sperm to facilitate pregnancy. However, 10%–20% of infertile men, who suffer from nonobstructive azoospermia (NOA), require surgical sperm extraction with procedures like microdissection testicular sperm extraction (microTESE) for ICSI.[2] The extract is a highly heterogeneous cell mixture with testicular tissues, and embryologists often spend up to 6–12 person-hours searching for rare sperm. Since background cells outnumber sperm by orders of magnitude, this tedious process is inefficient and often prone to error.[3,4] Intrauterine Insemination (IUI) is one of the most popular ARTs, which uses nonsurgical samples. These nonsurgical samples are comparatively larger and contain cellular debris that might render the process ineffective;[5] a sample needs to be purified and reduced in volume to increase the chances of successful fertilization.

Microfluidics, the technology of manipulating fluids in channels with scales ranging from tens to hundreds of micrometers, can promote optimization of sperm recovery rate from a microTESE sample. Applications pertaining to single-cell analysis and manipulation have been a significant driver for microfluidics advancement, thus leading to several research efforts for utilizing microfluidics in ART.[6] Some of the examples are the microfluidic solutions for conventional insemination, gamete manipulation, ICSI, and embryo culturing and monitoring.[6,7]

Microfluidic systems are reliable at isolating sperm for ART,[8] and a majority of these systems do not label the sperm while separating motile sperm from nonmotile sperm and debris.[9] The advantage of these microfluidic systems, which do not label the sperm, over other sperm recovery methods, which either label the sperm or use centrifugal force for separation, entails higher motile sperm yield without inducing any damage to the DNA.[9,10] However, the goal in the case of microTESE samples is to find a few nonmotile sperm, and the exclusion of nonmotile but viable

sperm renders these systems ineffectual. Also, for processing nonsurgical samples with a larger volume, as used in IUI, the throughput of a separation device being higher is preferred.

Previously, our group has developed microfluidic systems with a spiral channel for the isolation of low concentrations of low-motility sperm from red blood cells (RBCs),[11] and low concentrations of nonmotile sperm from white blood cells (WBCs).[12] While these systems worked well, they were not optimized and tested for maximum throughput and cell-separation performance.

Here, we introduce a microfluidic channel design with improved performance and throughput together with the theoretical modeling for further system optimization. The system utilizes inertial microfluidics,[13] which has found its application in the separation of particles based on shape and size. The unique shape and size of sperm compared to other cells enables them to be separated using the right microfluidic conditions. The key features of this system are the optimized spiral channel's hydrodynamic diameter (D_h), aspect ratio, and length. Our goal was to increase the system's sample processing rate and cell-separation performance while reducing the pressure drop through the channel. A secondary objective was to keep the pressure drop through the spiral as low as possible, as the high flow rates in a small channel occasionally lead to channel failure and leakage problems. The results show increased throughput for the system with moderate focusing of motile and nonmotile sperm and very sharp focusing of the RBCs. This design could be used to remove cellular debris, RBCs, and WBCs from nonsurgical larger samples used in IUI, as well as surgical samples, derived using microTESE.

II. DESIGN PRINCIPLE AND THEORETICAL MODELING

A. Theory

A substantial theory exists behind the physics of inertial microfluidics and flow-focusing of particles in spiral channels and was used to model, design, and optimize spiral channels for flow-focusing of sperm and blood cells. The channel dimensions and flow conditions were used to calculate important inertial microfluidic parameters such as the ratio of the inertial lift forces to the Dean drag force (R_f), the ratio between particle and channel dimension (λ), and the aspect ratio of the channel's cross section.[13–16] Particle focusing employing inertial microfluidics in a curved channel requires an equilibrium between inertial lift forces (F_L), which keeps particles away from the walls, and Dean drag (F_D), a lateral force generated by a secondary-vortex flow along the spiral channel's cross section. A balance can be reached for a given particle type when specific physical parameters of the flow are in specified ranges, and upon reaching that balance, different particles would focus at different equilibrium locations for their specific shape and size. In the case of blood cells and sperm, the equilibrium positions of blood cells lie toward the inner channel wall, while the sperm tend to focus away from the inner channel wall (Fig. 1). The net inertial lift force (F_L), the Dean drag force (F_D), and their ratio (R_f) can be calculated using[13,14]

$$F_L = 0.5\,\frac{a_p^4 \rho U_m^2}{D_h^2}, \tag{1}$$

$$F_D = 3\pi\mu U_D a_p = 5.4\times10^{-4}\,\pi\mu De^{1.63} a_p, \tag{2}$$

and

$$R_f = \frac{F_L}{F_D} \geq 0.04, \tag{3}$$

where a_p is the particle diameter, ρ is the density of the fluid, U_m is the maximum fluid velocity, D_h is the channel's hydrodynamic diameter, μ is the dynamic viscosity of the fluid, U_D is the average Dean velocity, and De is the Dean number.

For a particle to focus, R_f should be higher than 0.04,[14] which makes the Dean drag dominant, thus giving us the benefit of particle separation within a shorter channel length than in the case of a straight channel with no secondary flow. However, if the Dean drag is too significant, it would cause particles to continuously travel in a direction perpendicular to the channel flow, thus causing mixing instead of separation. For sharp focusing in a rectangular channel, the confinement ratio (λ) should be greater than or equal to 0.07, and it is given by[16]

$$\lambda = \frac{a_p}{H} \geq 0.07, \tag{4}$$

where H is the channel's shortest dimension, i.e., channel's height. The minimum channel length (L_f) required for a curved channel to result in flow-focusing of a particle is given by[16]

$$L_f = \frac{U_F}{U_L} \times L_M, \tag{5}$$

where U_F is the flow velocity, U_L is the lateral migration velocity of the particle, and L_M is the migration length. U_L and L_M are given as[16]

$$U_L = 0.5\frac{\rho U_m^2 a_p^3}{3\pi\mu D_h^2} \tag{6}$$

and

$$L_M = W + H + \frac{3}{4}W. \tag{7}$$

B. Theoretical modeling

Since effective removal of blood cells would result in the purification of sperm, calculations were performed using these theoretical principles to determine the channel size with the largest hydrodynamic diameter that would still facilitate a clear focusing of spherical particles of size 10 μm. We chose the 10 μm size because 9 μm and 12 μm spherical sizes have been used in our lab in the past to model RBCs and WBCs effectively.[11,12] Thus, 10 μm was assumed to be a good approximation to model the focusing behavior and position of blood cells. Similarly, 3 μm spheres have been determined to best model the ability of sperm to focus, though they do not focus on the same location as sperm.[12] Experimentally, it

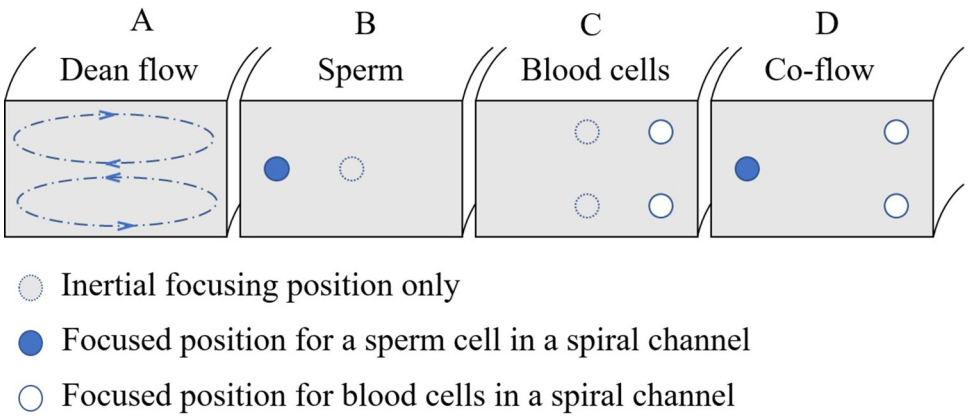

FIG. 1. Inertial-Dean flow-focusing in a rectangular curved channel. (a) Dean flow developed in a channel when the channel is curved. (b) Focusing behavior of sperm cells. The dotted circle represents the equilibrium position of a sperm cell in a straight channel. However, when the channel is curved, its equilibrium position shifts due to the Dean flow to the solid circle near the outer channel wall. (c) Focusing behavior of WBCs. The dotted circles represent the equilibrium positions in the absence of secondary flow, i.e., a straight channel, while the solid circles represent the equilibrium positions in the presence of the Dean flow, i.e., a curved channel. (d) Equilibrium positions of a sperm cell and WBC when flowing together in a curved channel. The figure shows how sperm cells shift toward the outer wall and WBCs shift toward the inner wall, resulting in separation from each other.

has been observed that sperm tend to focus to a position mirrored across the channel centerline from where the 3 μm spherical beads focus because of their highly asymmetrical shape including a tail almost 10 times longer than its body.

As a benchmark for comparison and improvement, we chose the largest channel system previously used for sperm and blood cell separation, a channel of size $600 \times 100\,\mu m^2$ with a hydrodynamic diameter of 1.71×10^{-4} m, as the reference device. Using the empirical formulas discussed above, values of R_f for 10 μm, 5 μm, and 3 μm sizes in different channel dimensions were plotted against different flow rates, while keeping the aspect ratios the same as the original 6:1. The flow rates were selected based on past experiments in the lab. From the theoretical modeling, it was found that a channel of size $800 \times 133\,\mu m^2$ with a hydrodynamic diameter of 2.28×10^{-4} m would be the maximum possible channel size to still result in a fully developed focusing for the 10 μm particles. This was an increase of 33% over the original hydrodynamic diameter. Figure 2 shows the comparison between the calculated values of R_f plotted against different flow rates for the two channel-sizes. For a channel of size $600 \times 100\,\mu m^2$, the values of R_f for 10 μm particles were observed to lie much above the minimum threshold of 0.04, which is required for a particle to focus in a curved channel clearly. This shows the potential for the channel size to be increased while still getting a precise focusing for the 10 μm size. For the calculated channel size of $800 \times 133\,\mu m^2$, the values of R_f for the particle size decreased to just above the minimum threshold of 0.04 required to focus in a curved channel.

Based on the calculations and the reference spiral-channel design, we designed our test device to be of size $800 \times 133\,\mu m^2$. The overall spiral channel had the smallest diameter of 20.4 mm, the largest diameter of 54 mm, a gap between turns of 0.8 mm, and 10 complete turns. The spiral channel was designed to have one inlet at the center and four uniformly divided outlets at the outer end of the channel. The outlets would be identified as 1 (innermost), 2 (inner), 3 (outer), and 4 (outermost), for convenience.

III. EXPERIMENTAL PROCEDURES

A series of experiments were designed to demonstrate the improved throughput of the spiral-channel device while maintaining the flow-focusing performance and resolution for particle separation.

A. Device fabrication

The designed device was fabricated using polydimethylsiloxane (PDMS, Sylgard 184, Dow Corning, MI, USA) with a SU-8 (SU-8 3035, Microchem, MA, USA) mold. A 100 mm (4 in.) silicon wafer was used to fabricate the SU-8 mold according to the manufacturer's instructions in a cleanroom environment. 50 ml of uncured PDMS base was mixed with 5 ml of curing agent and was poured over the mold after removing all the bubbles. The mold was then placed in an oven at 90 °C for 20 min. The molded PDMS was peeled off from the mold, and one inlet and four outlet holes were punched into the PDMS using a 1.5 mm diameter punching tool. The channel-side surface of the PDMS was cleaned and was plasma bonded to a clinical-grade glass slide (Thomas 6686M20, Thomas Scientific, Swedesboro, NJ), to form a closed channel. 1.5 mm silicone tubes were then fitted into the inlet and outlets to facilitate injection and collection of test samples.

B. Validation of theoretical models

Before testing the designed device with biological samples, a series of tests using 3 μm and 10 μm yellow-green polystyrene beads (Fluoresbrite®) was performed first to visualize the flow-focusing in the spiral and validate the theoretical models. One

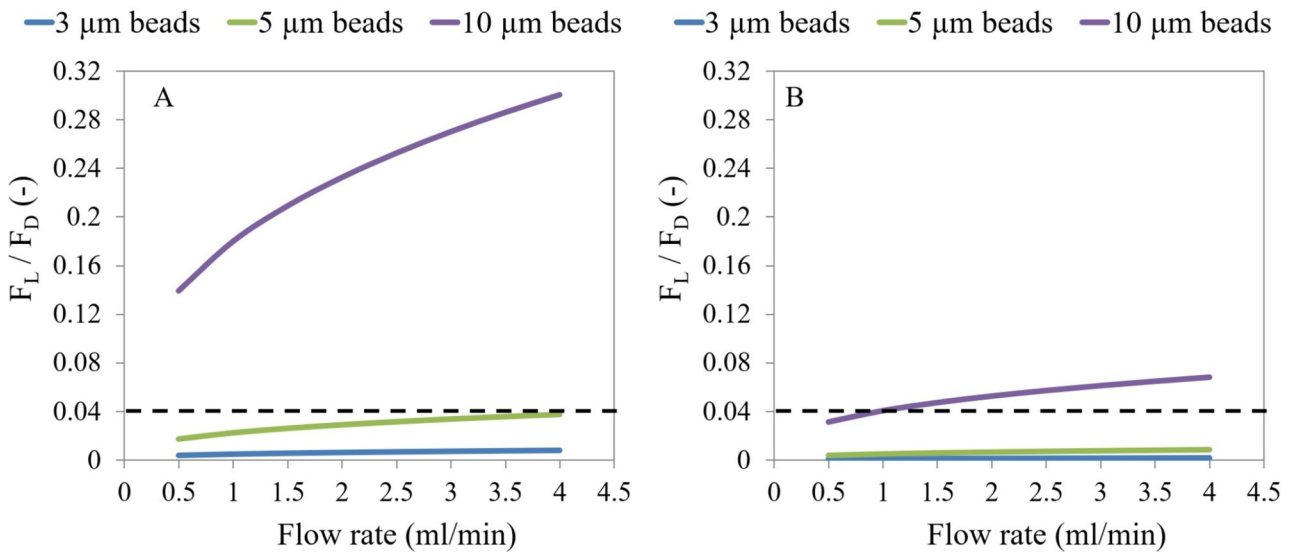

FIG. 2. Comparison of designs with an aspect ratio of 6:1. (a) R_f vs Q for the reference of size $600 \times 100\,\mu m^2$; $D_h = 1.71 \times 10^{-4}$ m. The values of R_f for the 10 μm particles were found to be much greater than the minimum theoretical threshold required for a developed focusing, i.e., 0.04, thus showing the possibility of further improvement. (b) R_f vs Q for a channel of size $800 \times 133\,\mu m^2$; $D_h = 2 \times 10^{-4}$ m. The values of R_f for the 10 μm particles were calculated to be just greater than the theoretical threshold for relevant flow rates.

undiluted drop of each bead was homogeneously suspended in 20 ml of de-ionized (DI) water separately. The device was placed on the stage of a confocal microscope, Nikon Eclipse Ti (Nikon Instruments Inc., Melville, NY, USA), with the microscope objective, focused at a point right before the outlet-junction [Fig. 6(a)]. 5 ml of a test sample was extracted using one 5 ml syringe, and it was injected into the middle inlet of the device at flow rates ranging from 0.5 to 3.5 ml/min with an interval of 0.5 ml/min using a programmable syringe pump. Higher flow rates were not tested since the secondary flow would be highly dominant beyond 3.5 ml/min, which was observed from the experiments, and also to prevent the device from leaking due to high pressure-drops. After stabilization of the flow, 250 images at 30 fps were taken at the focused point using NIS Elements software, and the images were stacked together to analyze the fluorescent intensity along the channel's width. The samples coming out of the four outlets were collected in a cup.

The projected images for each test were analyzed to get the fluorescence intensities plotted against the channel's width. The peak focusing position would then be identified using the location of the highest intensity in the intensity distribution along the channel width, and the focusing widths at half height of the intensity distribution would be measured and normalized for comparing focusing widths among different flow rates for each particle size. Since 10 μm particles would have a fully developed focusing, unlike 3 μm particles, the particle distribution along the width between the two would always be drastically different (with the 3 μm particles only slightly focused), thus making comparison among the two sizes ineffectual. So, the comparison was only made between distributions of the same particle size.

C. Experiments with sperm and RBCs

All sperm and RBC samples used in the experiments were acquired and used under IRB # 00093004. Previously frozen semen specimens suspended in sperm media [Quinn's Advantage media with HEPES (Sage, CT, USA) and 3% of serum protein substitute (Sage, CT, USA)] were used for preparing sperm samples, and RBC samples were obtained from donor's whole blood specimens within a day of collection, which mostly contained RBCs and small amounts of WBCs and platelets which could not be removed entirely. Sperm was extracted from its original media using density gradient centrifugation (DGC) and was later suspended and diluted to the ratio of 1:50 in sperm media for experimentation. RBC samples were suspended and diluted to the same ratio in sperm media separately. The dilutions of samples were done to reduce the cell concentrations to relevant levels. The original RBC and sperm samples were analyzed under a microscope using a hemocytometer. Images were captured, and the cells were counted for both samples. Table I provides the cell count data from the original samples.

After the sample preparation, 5 ml of each sample was drawn into 5 ml syringes separately. Two copies of the designed device were made for experimentation. The sperm sample was tested in one device and the RBC sample was tested in another device. To match the flow conditions with those used for the spherical beads, the experiments were first performed with the outlets at atmospheric pressure while a single inlet syringe was pushed at 3 ml/min into the middle inlet using the same programmed syringe pump. Then, a second protocol was run, based on experimental observations in the lab, to increase the recovery of sperm from the two outer outlets; four syringes were connected to the four outlets,

TABLE I. Sample details.

Sample type	Concentration of cells (10^6/ml)
RBC	1.5
Sperm	1.66

which were pulled at different flow rates with two programmable syringe pumps. The outer two syringes were pulled at 0.9 ml/min (30% of total flow rate each), and the inner two syringes were pulled at 0.6 ml/min (20% of total flow rate each), resulting in the total pull rate of 3 ml/min. The higher flow rate was used for the outer two outlet syringes to provide a higher pulling pressure for the sperm cells flowing into them, resulting in an increased sperm extraction. Finally, the number of cells in the collected samples of sperm and RBCs, from their respective devices, was counted using a hemocytometer.

IV. RESULTS AND ANALYSIS

A. Fabricated devices

Figure 3 shows the mold created by spinning and patterning SU-8 on a silicon wafer. After processing the SU-8, the resulting height of the channel was 130 μm instead of 133 μm, thus resulting in a decrease of the hydrodynamic diameter by less than 2%, which was considered to be negligible based on theoretical modeling.

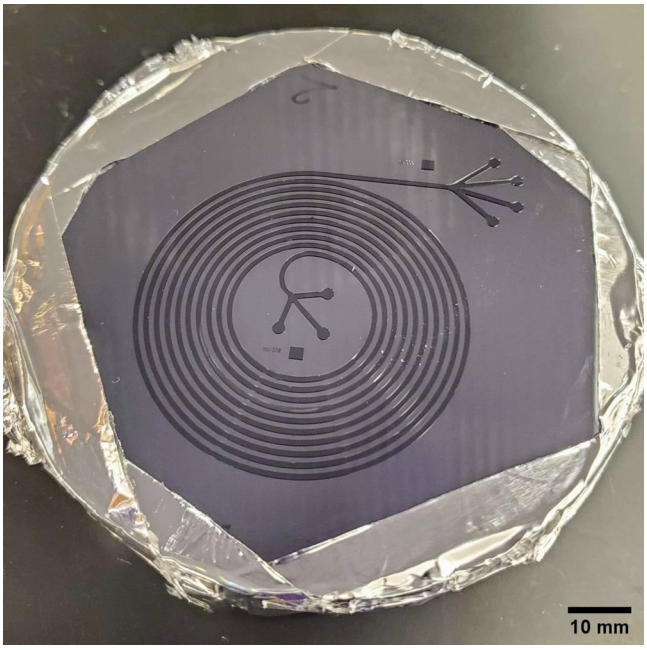

FIG. 3. A mold created by fabricating a SU-8 layer, with a design of the desired channel, on a Si-substrate.

B. Validation results

A comparison of intensity distributions obtained from the tests for 3 μm and 10 μm beads can be seen in Fig. 4, and the results obtained from the quantitative analysis of the images for focusing widths and focusing positions can be seen in Fig. 5. The 3 μm beads, because of their smaller size, experienced a relatively smaller amount of force for the same flow rate. So, the particles have poorer focusing in both devices.

In the case of 10 μm beads for the reference device, apart from the lowest flow rate of 0.5 ml/min, all higher flow rates resulted in sharp focusing [Fig. 4(a)]. Among the higher flow rates, the sharpest focusing was found to be at a flow rate of 2 ml/min [Figs. 4(a) and 5(a)]. In the case of 3 μm beads for the same device, the focusing width decreased from the flow rate of 0.5 ml/min to 1 ml/min [Figs. 4(c) and 5(a)]. The net inertial lift force would increase with the increase in flow rate, so the focusing widths started getting sharper for the higher flow rates. However, the Dean drag force eventually becomes dominant with higher flow rates. Thus, beyond the flow rate of 2 ml/min, the focusing widths started increasing significantly due to the increased Dean drag force, which in turn increased the mixing of particles. This mixing would consequently render these higher flow rates ineffectual for focusing and separation. At the best flow rate for the 10 μm particles, i.e., 2 ml/min, the focusing width for 3 μm particle was also observed to be very similar to the best result at 1.5 ml/min.

At the same flow rate of 2 ml/min, the focusing positions of 10 μm particles and the projected focusing positions of sperm cells, which would hypothetically lie opposite to the focusing positions of 3 μm particles, were also found to be far from each other [Fig. 5(b)]. The sharp focusing of the 10 μm particles at the flow rate of 2 ml/min would make their extraction more manageable, and, hypothetically, the separation resolution would easily separate sperm cells from WBCs. So, it could be inferred that the flow rate of 2 ml/min would be the better choice for their separation in a channel of size $600 \times 100\ \mu m^2$, and this is also the flow rate that is currently being employed in the group for this channel size.[17]

In the case of the designed device, the focusing widths of 10 μm beads were observed to be sharper with each increment in the flow rate, with the focusing being sharpest at the flow rate of 3 ml/min [Figs. 4(b) and 5(c)]. Beyond 3 ml/min, the focusing width was observed to be larger, and further tests were not performed to prevent device leakage due to a higher pressure drop in a comparatively longer channel. Similarly, for the 3 μm beads, the focusing width was the largest at the lowest flow rate of 0.5 ml/min, beyond which the widths were observed to decrease to acceptable widths [Figs. 4(d) and 5(c)]. At the best flow rate of 3 ml/min for the 10 μm particles, the focusing width for 3 μm particles was also found to be highest. Additionally, the focusing position of 10 μm beads at this flow rate was also observed to have a high separation resolution from the hypothetical focusing position of sperm, which was projected based on the focusing position of 3 μm beads [Fig. 5(d)].

Overall, coupling the focusing performance of both particles at the flow rate of 3 ml/min (a gain of 50% over the reference's flow rate of 2 ml/min) with the separation resolution in the designed channel, the designed device would result in increased throughput.

C. Optimization of the channel length

A channel's length is directly proportional to the pressure drop in the channel; this means that, when a fluid flows in a channel with a constant hydrodynamic diameter at a constant flow rate, a longer channel would require a larger pressure drop. After verifying that the designed channel size indeed resulted in increased throughput and proper separation of the particles, the next step was to try and reduce the length of the channel, which was ∼1.11 m. Reduction in the channel's length would allow us to operate the device with lower pressure requirements, which would also add to the device's reliability by reducing the chance of leakage. So, an optimum length was to be determined, which could still maintain the original focusing and separation resolutions of the beads at the flow rate of 3 ml/min.

From theoretical modeling, the minimum length required to achieve the mentioned goal was calculated to be ∼0.88 m. To accommodate for any possible discrepancies between the behavior of beads and cells, a tolerance of ∼10% was provided while

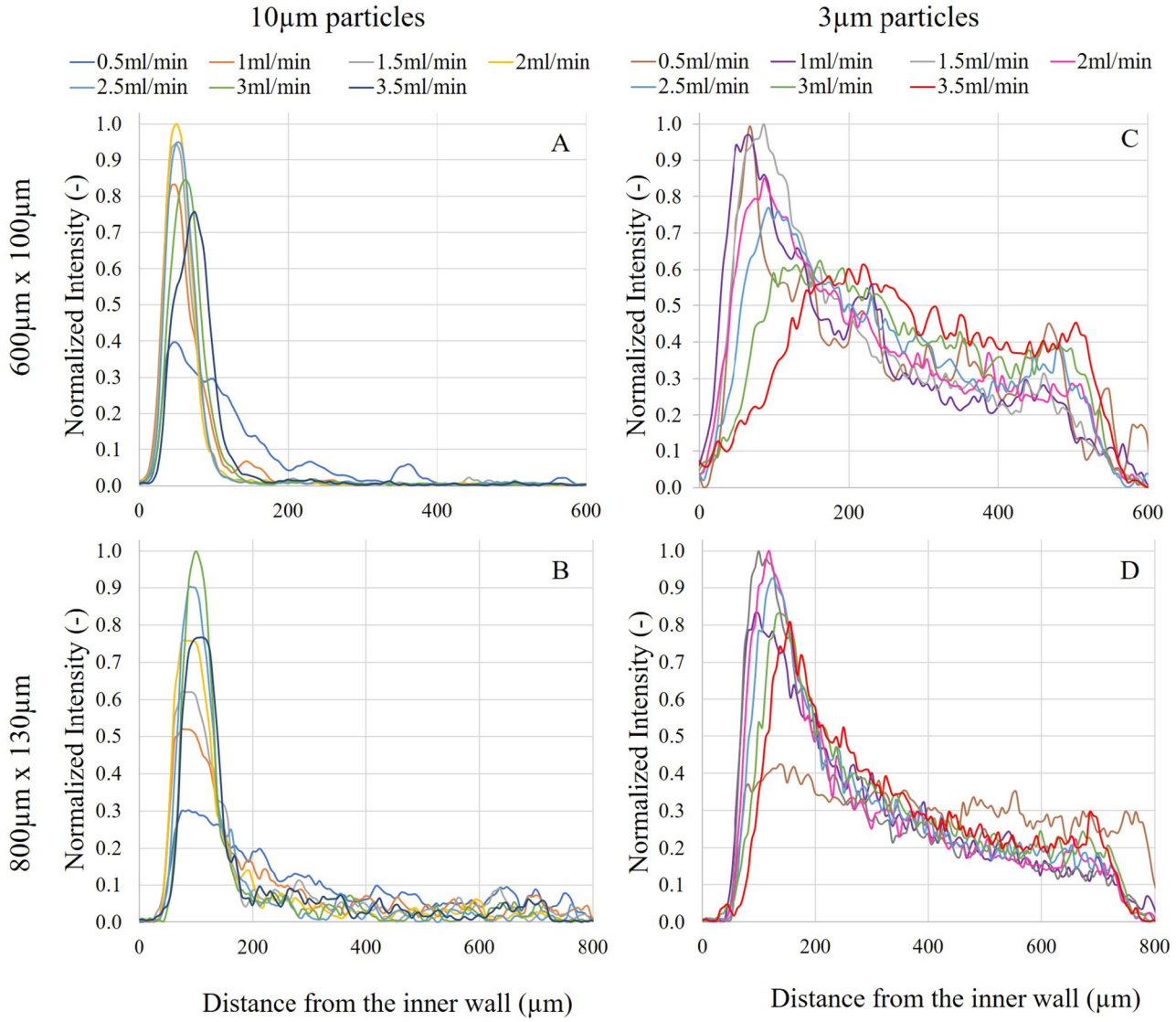

FIG. 4. Comparison of the designed channel to the reference. (a) and (b) are the plots showing the distribution of 10 μm beads at different flow rates in the reference channel (600 × 100 μm^2) and the designed channel (800 × 130 μm^2), respectively. As predicted from the modeling of the designed device, apart from the lowest flow rate of 0.5 ml/min, the focusing was still fully developed despite the increase in the channel size. (c) and (d) are plots showing the distribution of 3 μm beads at different flow rates in the reference channel (600 × 100 μm^2) and the designed channel (800 × 130 μm^2), respectively. It can be seen that the designed channel resulted in better focusing, although not fully developed, of the 3 μm beads at most of the higher flow rates.

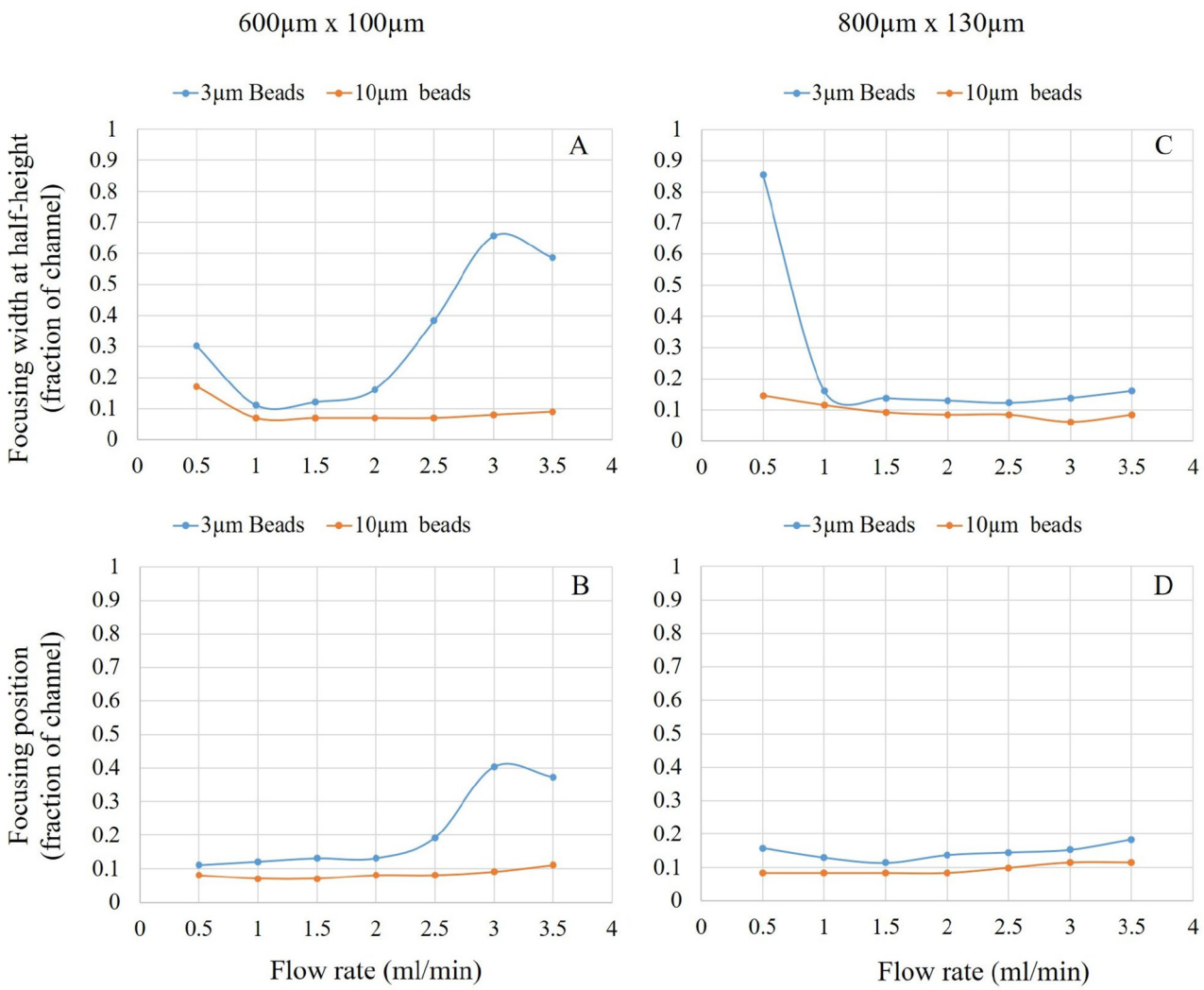

FIG. 5. Comparison of the analytical results obtained from the fluorescent images. (a) and (b) The calculated focusing widths and focusing positions of the particles in the reference device. The least focusing width for the 10 μm beads was observed at 2 ml/min; the flow rate also provided a reasonably good focusing width for the 3 μm beads. Experimentally, sperm tend to focus away from the focusing positions of spherical 3 μm beads because of the asymmetric shape, thus separating them from spherical or radially symmetric blood cells. (c) and (d) The calculated focusing widths and focusing positions of the particles in the designed device. The designed larger channel size increased the best flow rate for the 10 μm beads to 3 ml/min.

designing the experimental device, thus changing the channel length to about 0.96 m. This length was achieved by fabricating a new device that had its inlet at about where the third turn in the channel would start [Fig. 6(a)].

The results obtained from the modified device and the comparison of its performance to that of the unmodified device are shown in Fig. 6. First, to study the focusing behavior resulting due to the change in the channel's length, images were captured at position 1 for different flow rates [Fig. 6(a)]. The results of the images are shown in Figs. 6(b) and 6(c). It was observed that the device still demonstrated the best focusing performance at 3 ml/min.

After verifying that the performance was repeatable, images were also captured at two more positions (2 and 3), at a flow rate of 2.5 ml/min, to study how the focusing behavior would change with a further decrease in the channel length. The channel length in the case of position 2 was ~0.83 m, slightly lower than the theoretical value, and in the case of position 3, it was ~0.68 m. A lower flow rate of 2.5 ml/min was selected for these additional tests due to its performance being very similar to the flow rate of 3 ml/min [Fig. 6(b)].

Lengthwise comparison of the images captured at the multiple positions of the modified device to the image captured from the first device can be seen in Fig. 6(d). For the images taken at

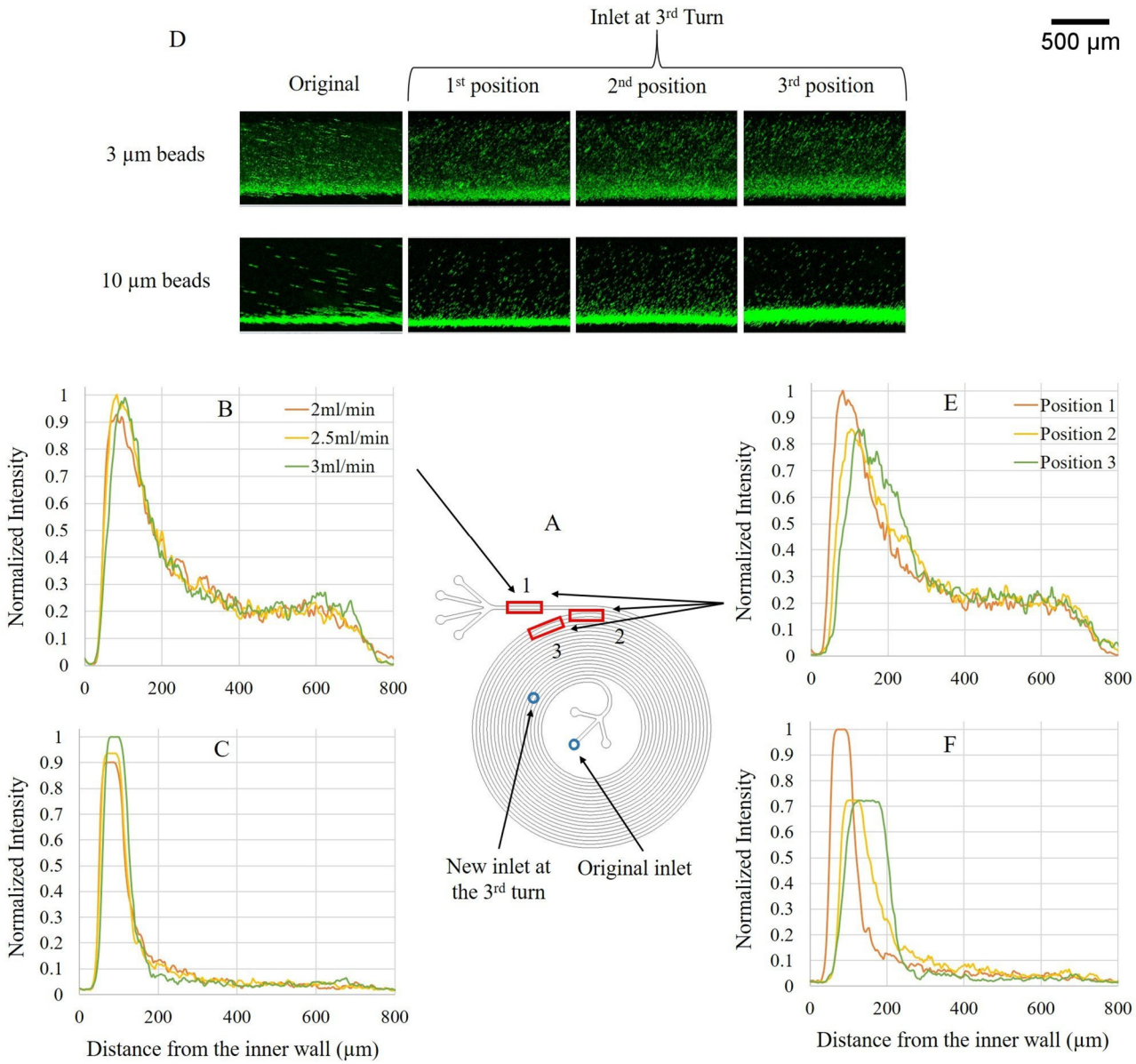

FIG. 6. Optimization of the channel length at the flow rate of 3 ml/min. (a) The channel design shows the points of inlet and the positions, 1, 2, and 3, where images of the flowing particles were taken. (b) and (c) Distribution of the 3 μm and 10 μm beads, respectively, at different flow rates in the optimized device. The images were taken at position 1. (d) Comparison of the experimental images obtained before and after changing the position of the inlet at the flow rate of 2.5 ml/min. (e) and (f) Distribution of the 3 μm and 10 μm beads, respectively, based on the images shown in (d). The focusing of both 3 μm and 10 μm beads can be seen to have been sharper in the successive outer turns. Also, the focusing positions slightly shifted toward the wall.

position 1, it can be observed that the results obtained before and after the reduction of channel length are not significantly different, implying no drastic change in the performance. Qualitative analysis of the images taken at different positions revealed that the focusing performances for both 3 μm and 10 μm beads were weaker in the inner positions, with the result being worse in the case of 10 μm beads [Figs. 6(e) and 6(f)]. For the 3 μm particles, position 3 resulted in the widest focusing, which would be the effect of shorter channel length. The focusing performance at position 2 was found to be sharper, and it was the sharpest at position 1. As expected, since the particle distributions still covered the channel's width, they were not fully developed. The focusing behavior for

TABLE II. The concentration of cells recovered from the four outlets using the first protocol.

	Concentration (10^6/ml)			
Samples	1 (Innermost)	2 (Inner)	3 (Outer)	4 (Outermost)
Sperm	0.365 (9.68%)	0.867 (23.01%)	1.400 (37.14%)	1.138 (30.17%)
RBC	5.985 (89%)	0.735 (10.9%)	0.005 (0.07%)	0.0025 (0.03%)

10 μm particles was also similar at all three positions, the difference being narrower and sharper focusing widths. By comparison, the particle focusing was not found to have been fully developed at positions 2 and 3. Also, the focusing positions at those two locations were found to slightly further away from the focusing position at the first location.

Nonetheless, since the focusing performance at position 2 was already getting narrower, there might be a possibility to

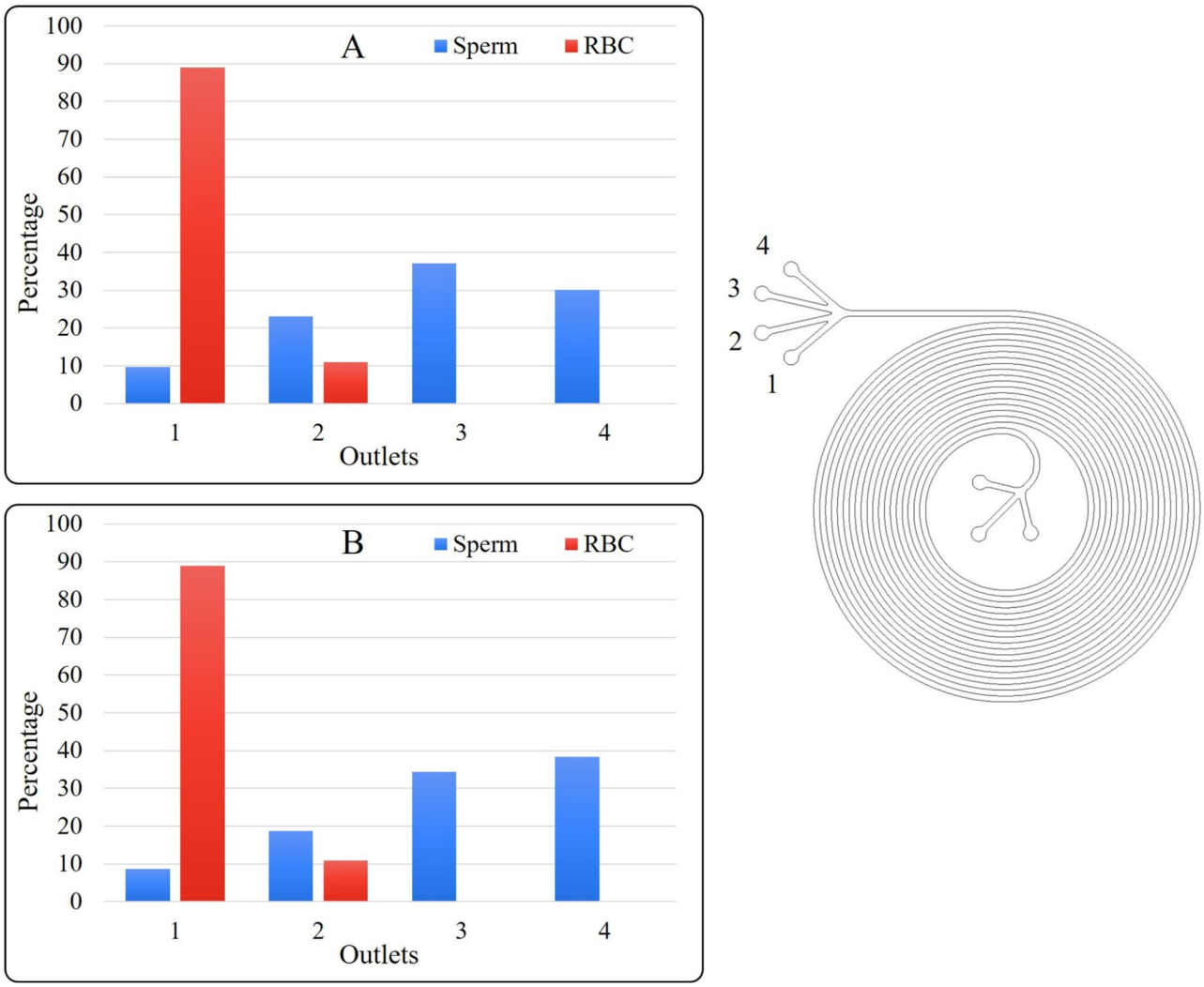

FIG. 7. Histograms showing the percentages of sperm and RBC samples collected from the four outlets while running (a) the first and (b) the second protocols. In each case, if sperm were recovered from the outer three outlets, it would result in a recovery of more than 90% of sperm while removing 89% of RBCs. The removal percentage would be higher for WBCs due to their larger size, spherical shape, and lower deformability. The second protocol would be a marginally better option to recover a higher percentage of uncontaminated sperm.

slightly lower the channel's length further while not losing the focusing performance and separation resolution. Additionally, it can also be observed that most of the 10 μm particles, even in the case of position 3, still fall within the inner one-third of the channel width. This means that if an original sample has enough sperm cells such that it can afford to lose the number of sperm cells lying in the innermost one-third of the channel and include the WBCs lying in the outermost two-thirds of the channel, the channel length of ~0.68 m can still be implemented for the separation process. In conclusion, the designed shorter channel length was considered to be close to the optimum length for achieving a fully developed focusing of 10 μm particles in the channel size. This length would be long enough to result in the best possible focusing for the larger sized particles with a proper separation resolution at the given flow rate for the channel size. Thus, it would ensure the removal of a high percentage of WBCs while losing a few sperm cells. However, if a sample can afford to lose sperm cells lying in the inner portion of the channel and can afford to include WBCs lying in the outer portion of the channel, the channel length can further be decreased to increase throughput and reduce pressure losses.

Overall, the optimized design had its internal diameter changed to 27 mm without losing the separation resolution significantly. This brought about 13.5% operational pressure reduction in comparison to the original design, thus resulting in a channel length that is only about 14% longer than the length of the reference channel size while resulting in an increase in the throughput by 50%.

D. Sperm and RBC test results

For our reference channel size of $600 \times 100\,\mu m^2$, 90% of sperm was recovered in the past while separating 74% of WBC. Table II shows the sperm and RBC concentrations obtained from the four different outlets together with the percentage distribution in comparison to the total output; Fig. 7 is the graphical representation of the data. As hypothesized, the sperm cells were mostly focused on the two outer outlets, with 67.3% of the total collected sperm lying within the outer 50% of the channel width, while 99.9% of collected RBCs were focused within the inner 50% of the channel width. Note that sperm focus away from the focusing positions of spherical beads, suggesting a shape-based effect that influences their focusing location. If sperm were collected from the three outer outlets, the result would be a recovery of more than 90% of sperm while removing 89% of RBCs, which is better than the results obtained for the reference device. The additional result obtained by implementing the second protocol is presented in Fig. 7(b). It was observed that using variable pulling pressures at the outlets increased the total sperm recovery from the outermost two outlets, thus making this protocol marginally better when recovering uncontaminated sperm is of utmost importance. Previous work by our group has shown the recovery rate of WBCs to be larger than that of RBCs due to their spherical shape and low deformability in flow-focusing;[12] this would mean that, on top of the increased throughput of 50%, the designed device would also result in improved separation of RBCs and WBCs from sperm.

V. CONCLUSION

In conclusion, we successfully designed a device to demonstrate an increase in throughput by 50% and also improved flow-focusing and separation performance in comparison to the reference to reduce RBC and WBC concentrations utilizing inertial microfluidic physics significantly.

Since an understanding of the physics behind particle focusing and separation in inertial microfluidics is still lacking, this work had to rely on the available literature to develop a theoretical model based on empirical formulas. Based on the model developed for inertial microfluidics in a curved channel, fairly reliable relationships between a channel size, its aspect ratio, hydrodynamic diameter, flow rate, particle size, and particle focusing behavior in the channel were identified. Based on the identified relations, the theoretical model helped determine the largest channel size that could result in a fully developed focusing of the 10 μm particles. After the design was built and tested to find the best flow rate for increased throughput, the theoretical model also proved useful in determining the minimum channel length possible while maintaining the same original focusing resolution.

Despite the theoretical model being useful in the mentioned two cases, there were still some areas where it was deemed wanting. Most importantly, the theory works based on flow rates and not velocity distribution, so it is unable to predict the exact focusing widths of the particles, and only does a qualitative analysis of a case where a fully developed flow-focusing occurs. In this work, even though the distribution of the 3 μm beads in the channel of size $800 \times 130\,\mu m^2$ was reasonably acceptable, the model predicted that the particles would not focus. So, the definition of "focused distribution" in a specific work might be different from what the model predicts. Additionally, even though it is known from the theory that the aspect ratio of a channel directly plays a significant role in determining the focusing positions, the model would not be able to predict the exact positions of differently sized particles in the channel at a given flow rate. This work had to rely on actual experiments to identify the focusing positions of particles in the channel.

Nonetheless, with some dependence on experimental modeling, the theoretical model was still successfully utilized to predict the performance of different channel-sizes, thus resulting in the design of a channel size with increased throughput and improved separation performance for sperm and blood cells. The improved device likely has application in ART and clinical treatments requiring the separation of sperm and blood, such as occurring in μTESE surgeries and leukospermia.

SUPPLEMENTARY MATERIAL

Please see the supplementary material for additional results from the theoretical modeling, and for the image analysis procedure employed in this work.

ACKNOWLEDGMENTS

The research reported in this publication was supported by the Eunice Kennedy Shriver National Institute of Child Health & Human Development of the National Institutes of Health under Award No.

R44HD095355. We would like to thank Raheel Samuel (Department of Mechanical Engineering, University of Utah, and Advanced Conceptions Inc.) for allowing us to use the company's lab.

DATA AVAILABILITY

The data that support the findings of this study are available within the article and its supplementary material. Additional data are available from the corresponding author upon reasonable request.

REFERENCES

[1]N. Kumar and A. Singh, J. Hum. Reprod. Sci. **8**, 191 (2015).
[2]C. Krausz, Best Pract. Res. Clin. Endocrinol. Metab. **25**, 271 (2011).
[3]R. Ramasamy, E. S. Fisher, J. A. Ricci, R. A. Leung, and P. N. Schlegel, J. Urol. **185**, 1394 (2011).
[4]R. Ramasamy, J. E. Reifsnyder, C. Bryson, N. Zaninovic, D. Liotta, C. A. Cook, J. Hariprashad, D. Weiss, Q. Neri, G. D. Palermo, and P. N. Schlegel, Fertil. Steril. **96**, 299 (2011).
[5]L. Gambera, F. Serafini, G. Morgante, R. Focarelli, V. De Leo, and P. Piomboni, Hum. Reprod. **22**, 1047 (2007).
[6]G. D. Smith and S. Takayama, Mol. Hum. Reprod. **23**, 257 (2017).
[7]S. M. Knowlton, M. Sadasivam, and S. Tasoglu, Trends Biotechnol. **33**, 221 (2015).
[8]R. Samuel, O. Badamjav, K. E. Murphy, D. P. Patel, J. Son, B. K. Gale, D. T. Carrell, and J. M. Hotaling, Syst. Biol. Reprod. Med. **62**, 161 (2016).
[9]T. G. Schuster, B. Cho, L. M. Keller, S. Takayama, and G. D. Smith, Reprod. Biomed. Online **7**, 75 (2003).
[10]W. Asghar, V. Velasco, J. L. Kingsley, M. S. Shoukat, H. Shafiee, R. M. Anchan, G. L. Mutter, E. Tüzel, and U. Demirci, Adv. Healthc. Mater. **3**, 1671 (2014).
[11]J. Son, K. Murphy, R. Samuel, B. K. Gale, D. T. Carrell, and J. M. Hotaling, Anal. Methods **7**, 8041 (2015).
[12]J. Son, R. Samuel, B. K. Gale, D. T. Carrell, and J. M. Hotaling, Biomicrofluidics **11**, 054106 (2017).
[13]H. Amini, W. Lee, and D. Di Carlo, Lab Chip **14**, 2739 (2014).
[14]D. Di Carlo, Lab Chip **9**, 3038 (2009).
[15]A. A. S. Bhagat, H. Bow, H. W. Hou, S. J. Tan, J. Han, and C. T. Lim, Med. Biol. Eng. Comput. **48**, 999 (2010).
[16]S. S. Kuntaegowdanahalli, A. A. S. Bhagat, G. Kumar, and I. Papautsky, Lab Chip **9**, 2973 (2009).
[17]A. Jafek, H. Feng, D. Broberg, B. Gale, R. Samuel, K. Aston, and T. Jenkins, Microfluid. Nanofluid. **24**, 60 (2020).